Coupling Perovskite Quantum Dot Pairs in Solution using a Nanoplasmonic Assembly

Elham Babaei, Demelza Wright, and Reuven Gordon – Hao Zhang, Parinaz Moazzezi, Juanjuan Ren, Brett Henderson, Christina Cordoba, Vishal Yeddu, Arthur M. Blackburn, Makhsud I. Saidaminov, Irina Paci, Stephen Hughes, and Reuven Gordon

2022

The final publication is available at:

https://doi.org/10.1021/acs.nanolett.2c01222

Citation for this paper:

Zhang, H., Moazzezi, P., Ren, J., Henderson, B., Cordoba, C., Yeddu, V., Blackburn, A. M., Saidaminov, M. I., Paci, I., Hughes, S., & Gordon, R. (2022). Coupling Perovskite Quantum Dot Pairs in Solution using a Nanoplasmonic Assembly. Nano Letters, 22(13), 5287–5293. https://doi.org/10.1021/acs.nanolett.2c01222

Coupling Perovskite Quantum Dot Pairs in Solution using Nanoplasmonic Assembly

Hao Zhang,[†,‡] Parinaz Moazzezi,[†,‡] Juanjuan Ren,[¶] Brett Henderson,[§,‡,‖] Cristina Cordoba,[⊥,‡] Vishal Yeddu,[§,‡] Arthur Blackburn,[⊥,‡] Makhsud I. Saidaminov,[†,‡,§] Irina Paci,[§,‡] Stephen Hughes,[¶] and Reuven Gordon[*,†,‡]

†*Department of Electrical and Computer Engineering, University of Victoria, Victoria, Canada*

‡*Centre for Advanced Materials & Related Technologies (CAMTEC), University of Victoria, Victoria, Canada*

¶*Department of Physics, Engineering Physics and Astronomy, Queen's University, Kingston, Canada*

§*Department of Chemistry, University of Victoria, Victoria, Canada*

‖*Quantum Algorithms Institute, Surrey, Canada*

⊥*Department of Physics and Astronomy, University of Victoria, Victoria, Canada*

E-mail: rgordon@uvic.ca

Phone: +1 (250) 472-5179. Fax: +1 (250) 721-6052

Abstract

Perovskite quantum dots (PQDs) provide a robust solution-based approach to efficient solar cells, bright light emitting devices, quantum sources of light. Quantifying heterogeneity and understanding coupling between dots is critical for these applications. We use double-nanohole optical trapping to size individual dots and correlate to emission energy shifts from quantum confinement. We were able to assemble a second

dot in the trap, which allows us to observe the coupling between dots. We observe a systematic red-shift of 1.1±0.6 meV in the emission wavelength. Theoretical analysis shows that the observed shift is consistent with resonant energy transfer and is unusually large due to moderate-to-large quantum confinement in PQDs. This demonstrates the promise of PQDs for entanglement in quantum information applications. This work enables future in situ control of PQD growth as well as studies of the coupling between small PQD assemblies with quantum information applications in mind.

Introduction

Perovskite quantum dots (PQDs) show intriguing properties for quantum technologies, such as bright and highly coherent single photon emission,[1] and superfluorescence in ensembles of dots.[2] Coupled quantum dots have long been investigated for quantum computing.[3,4] Many fabrication strategies have been proposed to couple different types of quantum dots, not only PQDs.[5–10] Assembling quantum dots and studying their quantum coupling in solution would greatly simplify such studies. Furthermore, by assembling in solution, it is possible to study the individual dots prior to assembly, and then study the impact of coupling in the near-field, which is not possible with pre-assembled pairs.

Studying individual dots also allows for probing non-uniformity of the PQDs in solution. Uniformity has been recognized as an important parameter for high-performance applications.[11–17] For solar cells, monodisperse PQDs have shown higher conversion efficiencies and open circuit voltages.[18] PQDs are recognized as highly coherent single photon emitters;[1] however, for indistinguishable photons, nearly-identical emitters are desired and this requires a way to select among individual emitters in the ensemble.[19,20] Past efforts have focused on ex-situ characterization (e.g., transmission electron microscopy – TEM) of already synthesized PQDs. Ideally, particle size would be monitored in solution in real time, allowing for in-situ tailoring of growth conditions while preventing degradation from exposure to the environment.

Here, we use double-nanohole (DNH) optical tweezers to characterize the dispersion of cesium lead bromide ($CsPbBr_3$) PQDs and their coupling in solution. Aperture based optical tweezers have been used to trap quantum dots,[21] study their emission (also with two photon excitation),[22] and enhance their single photon emission characteristics.[23] We demonstrate that the DNH optical tweezer can be used to determine the sizes of individual PQDs and correlate size with the emission spectra shifts from quantum confinement. We also demonstrate that the DNH tweezer can capture two quantum dots (i.e., assemble them in real-time) and thereby measure the spectral shift that arises from their coupling. Therefore, this platform enables the spectral and size characterization of single and double dots, and most importantly, it achieves this feat in-situ without removing the dots from the solution or requiring electron microscopy that would damage them.

Multiple physical mechanisms can be responsible for quantum dot coupling in solution. For quantum dots that are nominally symmetric and do not allow for electron tunneling, Förster resonant energy transfer (RET) has been considered as a way to achieve coupling between dots, providing a possible avenue towards quantum information processing.[24] In the past, RET has been studied for PQDs of different sizes, where the longer wavelength emission peak is enhanced due to one-directional energy transfer.[25] The bi-directional coupling that arises from just two PQDs that are nominally the same size has not been investigated so far.

Results and discussion

Heterogeneous Particle Sizing

$CsPbBr_3$ PQDs were synthesized by the ligand-assisted reprecipitation technique.[26] The side-length distribution was calculated by averaging over 150 PQDs. Also shown is the distribution of smallest edge sizes, since the PQDs are expected to align along their long sides when pushed together by optical forces, and so the separation is best represented by their small side size. We find the small side size to be 10.5 $\pm$ 1 nm, as shown in the

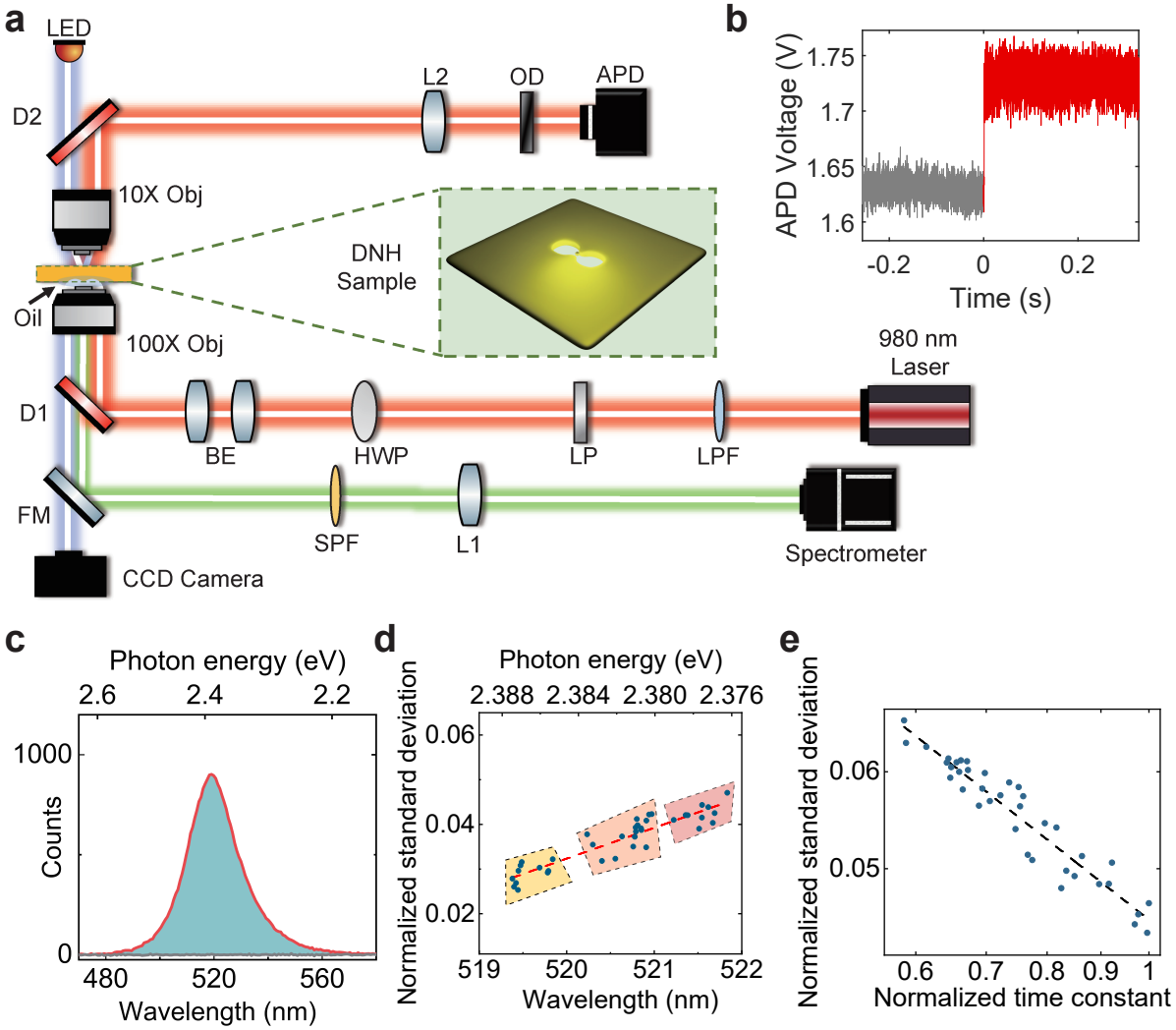

Figure 1: (a) Optical trapping setup: long pass filter (LPF), linear polarizer (LP), half-wave plate (HWP), beam expander (BE), dichroic mirror (D), objective lens (Obj), lens (L), optical density filter (OD), avalanche photodetector (APD), flip mirror (FM), short-pass filter (SPF), charge-coupled device (CCD). (b) Single trapping event (untrapped: grey, trapped: red). (c) Emission in situ (untrapped: grey, trapped: red) . (d) Relation between emission wavelength and standard deviation of trapping laser transmission for individual trapped PQDs. Three groups of the sample were measured. This shows that the standard deviation can be used as an independent measure of the particle size, which correlates well with the quantum confinement induced blue-shift. (e) Standard deviation against autocorrelation time constant (τ) of the single quantum dots trapping events on log-log plot. The slope for the best linear fit is about -0.68.

Supporting Information (SI), Fig. S1; however, this size showed variation of 0.5 nm between separate fabrication runs. We diluted the sample with toluene 20-fold, then placed the solution in a microwell formed by an imaging spacer (Grace Biolabs) on a slide 0 coverslip. A gold film containing DNHs on glass, fabricated using past approaches,[27] was placed on top of the microwell to seal. We then placed the sample in an inverted microscope optical tweezer setup adapted from a modular kit (Thorlabs – OTKB), shown in Fig. 1a, which has been used previously to study lanthanide nanocrystals.[28,29] The modified setup included a spectrometer for measuring the spectrum of PQD(s) in the DNH optical tweezer. The excitation of the PQD was obtained by a two-photon process, since the laser wavelength was 980 nm (1.26 eV), and the emission wavelength was 520 nm (2.38 eV). Two photon excitation of colloidal quantum dots has been observed previously in trapping setups.[22,30] We confirmed the two-photon process by the quadratic power dependence, as outlined in the SI, Figure S4. The observed wavelength is similar to past works for similarly sized dots,[1] but longer than smaller perovskite dots.[11]

A step in the transmission of the laser through the DNH was seen with trapping as shown in Fig. 1b. This step resulted from the dielectric loading of the DNH by the PQD, which made the aperture optically "bigger". Several works have confirmed that the single step is the result of an individual nanoparticle being trapped, e.g., by using fluorescent particles[31] or by noting the dynamics when multiple particles are trapped.[32] The spectrum of the single dot is shown in Fig. 1c, which was recorded after the trapping occurred. There was no emission observed before trapping.

It was possible to estimate the size of each isolated trapped PQD by analyzing thermal motion induced fluctuations. As demonstrated previously for proteins (but not for PQDs), the autocorrelation time of the thermal motion scales as γ/κ, where γ is the drag coefficient (which scales as the cross sectional width in the viscous limit) and κ is the optical tweezer stiffness (which scales as the volume of the particle in the dipole limit). Therefore, for radius r, $\tau \propto r^{-2} \propto \Omega^{-2/3}$,[33,34] where Ω is the volume. Also, the standard deviation of the

light scattering scales linearly with the size.[34] This has been applied to study heterogeneous solutions of proteins.[35] Here we apply it to sizing individual PQDs and correlating the size with the emission spectrum shifts from quantum confinement.

Fig. 1d shows the standard deviation of the trapping laser fluctuations correlated with the emission wavelength for individual PQD trapping events. This data was taken from three separate batches, and shows a clear separation in the sizes of these batches. As described above, it is expected that the standard deviation scales linearly with particle size. For small (first-order) variations in size, it is also expected that the wavelength scales linearly with particle size. Therefore, we observe a linear relationship between the standard deviation and the emission wavelength. We considered the autocorrelation time as a separate measure of particle size, as shown in Fig. 1e. We observed that the relation between the standard deviation and the autocorrelation time had a -0.68 slope on a log-log plot, where a slope of -2/3 is the theoretical prediction.[34] The detailed calculation is shown in the SI.

The size-dependence of the emission spectra of individual PQDs can be modeled by solving the Schrödinger equation under the effective mass approximation.[36] While spherical particles with infinite barriers allow analytical calculations,[36] here we also use numerical calculations which allows for cubic particles and finite barrier energies.[37] Details of the calculation method are provided in the SI. The ability to size and spectroscopically characterize individual dots in solution is relevant for quantum applications where we seek to obtain multiple indistinguishable emitters.[1] The method can also be used in-situ to optimize solution-based growth.[14–17,38]

Two Quantum Dot Assembly via Trapping (Dimers)

The trapping setup allowed us to measure and characterize the quantum coupling between two PQDs assembled in real time and isolated in the trap. We observed two steps corresponding to double PQDs trapped subsequently in the same aperture as shown in Fig. 2a. It has been shown in past works on aperture optical tweezers that the co-trapping of two

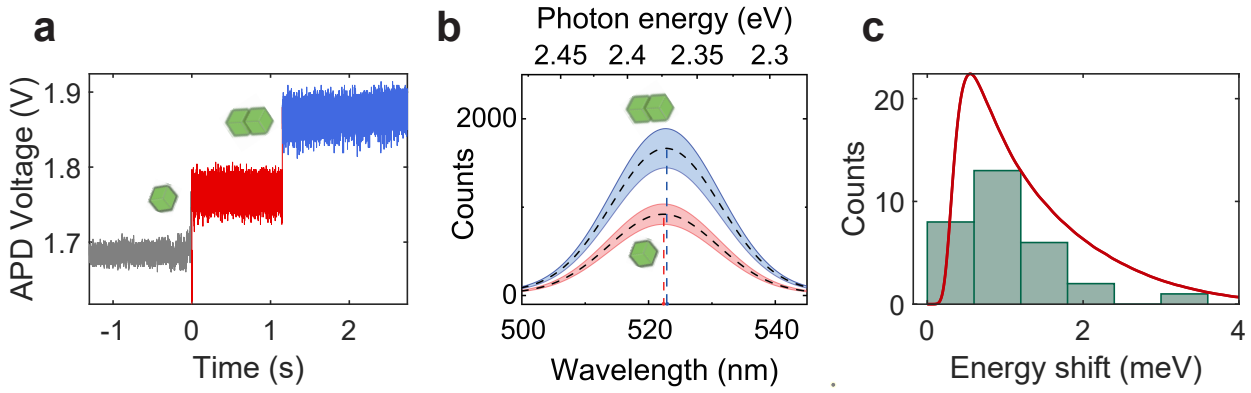

Figure 2: (a) Double trapping event collected by APD (first trapping: red; second trapping: blue). (b) Spectra of single dot trapping and double dot trapping are shown in red and blue. The areas filled with blue and red stand for the experiment data (fitted) at each sampling time. Black dotted lines indicate the average of the varying spectra region (quantum blinking). (c) Experimental (green bars) and simulated (red curve) energy shift upon coupling. Experimental values were observed among 30 different DNHs, each measured at least 6 times, and the simulation represents the energy shift by Förster interaction between two dots randomly selected from 1000 dots (normal distribution).

nanoparticles results in a double step profile.[32] Fig. 2b shows the observed distribution of emission for single and double PQD trapping averaged over 30 different DNHs, averaging over at least 6 measurements at each DNH (full data is included in the SI, Figure **??**). Fig. 2b, shows that the emission intensity approximately doubled when there are two PQDs, and that there was a systematic spectral red-shift of the emission. Fig. 2c quantifies the systematic red-shift in the emission observed for the multiple double-dot trapping events. It is relevant to note that there was always a red-shift: if the energy was simply transferred from the smaller dot to the larger one (as is the case for past works on RET[25]), we would expect on average a red-shift sometimes and no shift at other times, depending on whether a smaller or a larger dot was trapped first.

Before discussing the physical mechanism that may be responsible for this red-shift, let us describe a simple generic model for the energy shift arising from a generalized coupling potential V. Considering two oscillators with energies E_1 and E_2, the shift from E_1 upon

coupling can be calculated as:[24,39]

$$\Delta = \frac{1}{2}\left[(E_2 - E_1) - \sqrt{(E_1 + E_2)^2 - 4(E_1 E_2 - V^2)}\right]. \tag{1}$$

Fitting Δ to the observed shift, we find a best fit for $V = 1.1$ meV, as shown in Fig. 2c.

Coupling Mechanisms Between Perovskite Quantum Dots

We now discuss a possible physical mechanism underlying the observed systematic spectral red-shift. First, we discuss the expected photon coupling between two PQDs, treated as point dipoles. As shown in the SI, the *radiative* decay rate from a single dipole emitter is

$$\Gamma_1(\mathbf{r}_1) = \frac{2\mathbf{d}_1 \cdot \mathrm{Im}\{\mathbf{G}(\mathbf{r}_1, \mathbf{r}_1, \omega)\} \cdot \mathbf{d}_1}{\epsilon_0 \hbar}, \tag{2}$$

for an emitter with dipole moment $\mathbf{d}_1$ (assumed real) at position $\mathbf{r}_1$, and $\mathbf{G}$ is the photon Green function, for any generalized medium. For coupled dipoles, the photon exchange has real and imaginary parts, defined through the incoherent rates of photon transfer:

$$\Gamma_{12} = \frac{2\mathbf{d}_1 \cdot \mathrm{Im}\{\mathbf{G}(\mathbf{r}_1, \mathbf{r}_2, \omega)\} \cdot \mathbf{d}_2}{\epsilon_0 \hbar}, \tag{3}$$

and a coherent exchange term

$$\Delta_{12} = -\frac{\mathbf{d}_1 \cdot \mathrm{Re}\{\mathbf{G}(\mathbf{r}_1, \mathbf{r}_2, \omega)\} \cdot \mathbf{d}_2}{\epsilon_0 \hbar}. \tag{4}$$

The latter gives rise to spectral frequency shifts through photon exchange.

When one considers a homogeneous medium (with $\epsilon_b = n_b^2$ using two dipoles spatially separated by $r_{12} = 11$ nm (center to center), and in the near-field regime, then the coherent

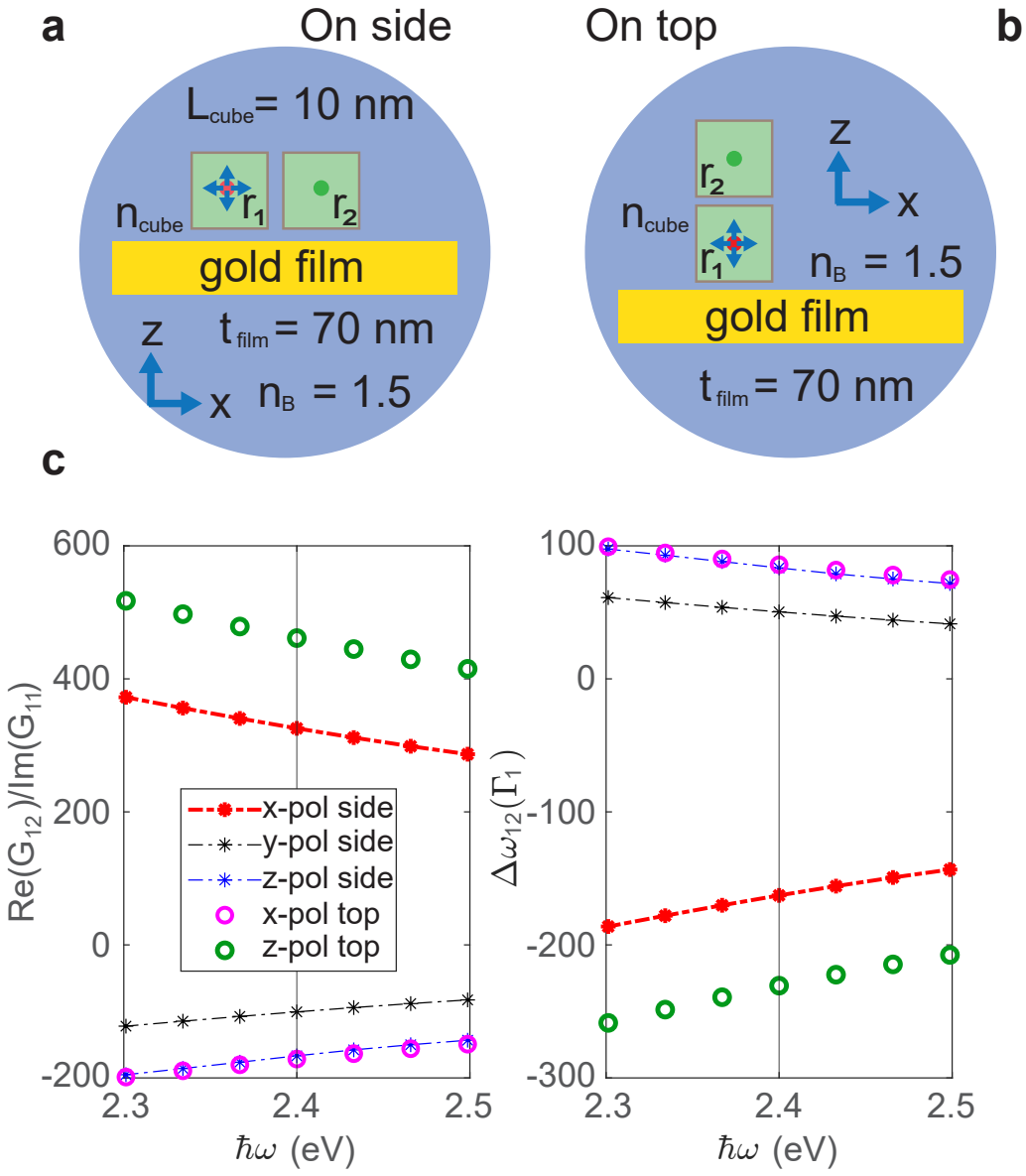

Figure 3: Schematic diagram for PQD dimer with (a) side coupling (left) or (b) top coupling (right). PQDs are shown in green in the two figures. (c) Example calculations for the propagators and dipole-dipole shifts computed from COMSOL, which includes the full scattering geometry. We show different dipole polarizations, and dipole-dipole coupling for PQD cubes that are horizontally stacked or vertically, and separated by 1-nm. All terms include local field corrections, so are normalized by the result including the single PQD cube.

exchange term, with s-polarized dipoles, is

$$\hbar\Delta_{12}^{ss} = \frac{d^2}{4\pi\epsilon_0\epsilon_b r_{12}^3} \approx 93\,\hbar\Gamma_1 = 0.25 \text{ meV}, \tag{5}$$

while for p-polarized dipoles,

$$\hbar\Delta_{12}^{pp} = -\frac{d^2}{2\pi\epsilon_0\epsilon_b r_{12}^3} \approx -186\,\hbar\Gamma_1 = -0.50 \text{ meV}, \tag{6}$$

where we have used $d = 0.72\,\mathrm{e}\cdot\mathrm{nm}$ and $\epsilon_b = 1.5^2$, yielding a nominal radiative decay rate of $\hbar\Gamma_1 \approx 2.69$ μeV (corresponding lifetime of 250 ps); this estimate scales with $\Gamma_{1,2}$ so could easily be larger. Note that these analytical rates identically recover the well known Förster coupling terms, and can be described semi-classically or quantum mechanically. Below, we will introduce the shorthand notation $\mathbf{G}_{12} = \mathbf{G}(\mathbf{r}_1, \mathbf{r}_2)$. For identical dipole emitters, the resonance will split by $\pm\hbar\Delta_{12} \equiv \pm V_F \propto \mathrm{Re}\{G_{12}\}$, into subradiant and superradiant states, where the latter is optically bright. ($V = V_F$ for RET in Eq. (1)).

In the SI, we describe how these radiative decay and exchange rates are influenced by local field corrections and interactions with the metal film, from both an analytical perspective as well as using full numerical simulations in COMSOL. As an example of the latter calculations, here we consider two PQD cubes placed 1 nm above a gold film, either horizontally coupled or vertically coupled, as shown in Figs. 3a and b. The PQD cubes are separated by 1-nm (gap size), and various dipole polarizations are considered. The corresponding Green function propagators and dipole-dipole coupling rates (in units of the radiative decay rate) are shown in Fig. 3c. Overall we predict that at $\hbar\omega = 2.4$ eV, maximum photon exchange rates of around $-231\hbar\Gamma_1$ are possible, which we estimate to be around -0.62 meV (for z-polarized dipoles with top coupling).

After initial calculations at a 1 nm gap size, we obtained a more accurate measurement of the gap size from high-resolution TEM as being 1.4 nm. This has a small (10%) impact on the theoretical values (Fig. S12). The typical gap for oleic acid PQDs in TEM imaging is

between 1 and 2 nm.[1,2,26,40?] The optical force tends to squeeze the particles together and minimize the gap size in solution, and so we expect this is similar to what was observed by HR-TEM, although it is possible that it is slightly larger due to the presence of the solvent and thermal motion.

It is also important to note that the expected exciton Bohr radius is much smaller than the size of the PQDs, which gives rise to a giant oscillator strength for an optical transition.[41,42] This is caused by a correlated exciton wave function that affects both the radiative decay and the dipole-dipole coupling rates. We discuss and estimate this enhancement in the SI, which we expect to be about a factor of 5 bigger than PQDs in the strong confinement regime. This is significant, even in the presence of local field reductions. Also in the SI, we discuss several other possible coupling mechanisms including Dexter coupling, electronic tunneling, exciton tunneling for fused dots, and possible monopole-monopole interactions.

Discussion

In-Situ Real-Time Size-Spectral Characterization

In the present work, we have demonstrated the use of an optical tweezer platform to characterize multiple individual PQDs in solution. In past works, the standard approach for monitoring PDQ synthesis has been to follow up PDQ growth with characterization via TEM or luminescence studies. Here we show that we can accurately determine the size and the spectral response without the need for TEM. This may allow for fine-tuning or improving growth conditions in-situ. For example, it is possible to envision integrating the present trapping setup with a flow-cell [21] for real-time monitoring and/or modifying of growth conditions.[38]

Quantum Dot Coupling

We believe that RET is the dominant coupling mechanism between the two PQDs. We do not think the observation can be explained by other mechanisms, like Dexter coupling and quantum hybridization, because the barrier height is too large and the gap too wide to allow substantial tunneling.[43] RET has been observed in ensembles of dissimilar PQDs;[25] however, that exchange is uni-directional (from the higher energy to the lower energy PQD). Here, since the dots are nominally the same size, the exchange is bidirectional. For quantum applications, RET has been proposed theoretically as a mechanism to achieve quantum computing via colloidal quantum dots.[24] Here we estimate the magnitude of the RET induced shift. The dipole moment is estimated from previously reported values of the emission lifetime. We further note that the PQDs studied here are large relative to the exciton Bohr radius, and are in the intermediate to weak confinement regime. This enhances the strength of the RET interaction by 5 times with respect to strongly confined dots, which is a particularly relevant finding of this work.

We estimate from a dipole model that the shift is at least two orders of magnitude larger than the radiative lifetime. We have also looked at distributed wavefunctions (beyond the local dipole model), and full COMSOL simulations including the metal surface nearby in aperture, and these only provide small corrections to the value reported above (as described in the SI). Since this value is comparable to what we observed in the experiments, RET is a plausible explanation for the observed shift. In the future, we aim to modify the ligands and the dot size to investigate their impact on the RET, since there is a strong size-dependence of this effect.

Conclusions

We have demonstrated the ability to characterize the size and coupling between individual and dimer PQDs in solution, and simultaneously observe their emission spectra using

nanoplasmonic tweezers. This is a powerful tool to quantify sample heterogeneity in size and emission in solution, without requiring expensive and damaging techniques. The approach may be extended to isolate identical dots (both in terms of size and spectral emission), which is a pathway to achieving indistiguishable quantum emitters. The approach may also be extended to monitor and modify growth in real time.

We quantified the systematic red-shift for coupled PQDs in solution of 1.1 $\pm$ 0.6 meV and we argue that this is likely the result of resonant energy transfer. The magnitude of the RET is unusually large when compared with the strongly confined quantum dots that have been explored in the past, which is intriguing because RET has been proposed as a mechanism to obtain entanglement for quantum information processing applications.[24]

In the future, We aim to consider the impact of temperature on the observed spectral shifts, which will require adding cyrogenic capability to our setup so that the temperature can be lowered after trapping is achieved. To first order, RET does not depend on temperature,[? ?] however, more advanced electron-phonon theories predict a renormalization of V_F as a function of temperature.[? ?] We present only a simple temperature independent model here, as a first order quantification of the RET effect. It may be possible to modify the setup to allow for cryogenic cooling after trapping is achieved, and for time-resolved ultra-fast probing of the trapped dots. Combined, these advances will allow for further exploration of the coupling between these quantum emitters. The DNH optical tweezer is an interesting platform for studying regimes of coupling for small assemblies of 2 or more PQDs (however larger apertures would be preferred for multiple dots). In this manner, it may be possible to explore the full range of interactions from the single dot, coupled dots, several dots, to large cluster superfluorescence ensemble measurements;[2] thereby transitioning from the nanoscopic to mesocopic regimes.

Acknowledgement

The authors thank the NSERC CREATE in Quantum Computing program and the fabrication facilities of CAMTEC. We also acknowledge NSERC for funding through the Discovery Grants program, the Canadian Foundation for Innovation (CFI) for computational infrastructure funding through the Innovation Fund, and CMC Microsystems for the provision of COMSOL Multiphysics.

Declarations

The authors declare no competing interests.

Contributions

H.Z. fabricated the DNHs, performed the trapping experiments, analyzed the data and did the FDTD simulation. P.M. and V.Y. made the PQD samples. M.I.S. advised on PQD synthesis and characterization. C.C. and A.B. were responsible for TEM imaging. B.H. and I.P. contributed to simulation of bandgap and emission energy as a function of single PQD size. J.R. and S.H. contributed to the theory and simulations of coupled quantum dots. R.G. advised on the experiments and analysis. All authors contributed to writing the manuscript.

Supporting Information Available

Fabrication details, detailed optical trapping description, bandgap and emission characteristics of PQDs, and theory and simulations of coupled quantum dots.

References

(1) Utzat, H.; Sun, W.; Kaplan, A. E.; Krieg, F.; Ginterseder, M.; Spokoyny, B.; Klein, N. D.; Shulenberger, K. E.; Perkinson, C. F.; Kovalenko, M. V., et al. Coherent single-photon emission from colloidal lead halide perovskite quantum dots. *Science* **2019**, *363*, 1068–1072.

(2) Rainò, G.; Becker, M. A.; Bodnarchuk, M. I.; Mahrt, R. F.; Kovalenko, M. V.; Stöferle, T. Superfluorescence from lead halide perovskite quantum dot superlattices. *Nature* **2018**, *563*, 671–675.

(3) Burkard, G.; Loss, D.; DiVincenzo, D. P. Coupled quantum dots as quantum gates. *Physical Review B* **1999**, *59*, 2070.

(4) Loss, D.; DiVincenzo, D. P. Quantum computation with quantum dots. *Physical Review A* **1998**, *57*, 120.

(5) Kim, D.; Carter, S. G.; Greilich, A.; Bracker, A. S.; Gammon, D. Ultrafast optical control of entanglement between two quantum-dot spins. *Nature Physics* **2011**, *7*, 223–229.

(6) Rodary, G.; Bernardi, L.; David, C.; Fain, B.; Lemaître, A.; Girard, J.-C. Real space observation of electronic coupling between self-assembled quantum dots. *Nano Letters* **2019**, *19*, 3699–3706.

(7) Koley, S.; Cui, J.; Panfil, Y. E.; Banin, U. Coupled colloidal quantum dot molecules. *Accounts of Chemical Research* **2021**, *54*, 1178–1188.

(8) Panfil, Y. E.; Shamalia, D.; Cui, J.; Koley, S.; Banin, U. Electronic coupling in colloidal quantum dot molecules; the case of CdSe/CdS core/shell homodimers. *The Journal of Chemical Physics* **2019**, *151*, 224501.

(9) Cui, J.; Panfil, Y. E.; Koley, S.; Shamalia, D.; Waiskopf, N.; Remennik, S.; Popov, I.; Oded, M.; Banin, U. Colloidal quantum dot molecules manifesting quantum coupling at room temperature. *Nature Communications* **2019**, *10*, 1–10.

(10) Cassidy, J.; Yang, M.; Harankahage, D.; Porotnikov, D.; Moroz, P.; Razgoniaeva, N.; Ellison, C.; Bettinger, J.; Ehsan, S.; Sanchez, J., et al. Tuning the Dimensionality of Excitons in Colloidal Quantum Dot Molecules. *Nano Letters* **2021**, *21*, 7339–7346.

(11) Krieg, F.; Sercel, P. C.; Burian, M.; Andrusiv, H.; Bodnarchuk, M. I.; Sto**********ferle, T.; Mahrt, R. F.; Naumenko, D.; Amenitsch, H.; Raino**********, G., et al. Monodisperse long-chain sulfobetaine-capped CsPbBr3 nanocrystals and their superfluorescent assemblies. *ACS central science* **2020**, *7*, 135–144.

(12) Tennyson, E. M.; Roose, B.; Garrett, J. L.; Gong, C.; Munday, J. N.; Abate, A.; Leite, M. S. Cesium-incorporated triple cation perovskites deliver fully reversible and stable nanoscale voltage response. *ACS Nano* **2018**, *13*, 1538–1546.

(13) Bhattacharyya, S.; Rambabu, D.; Maji, T. K. Mechanochemical synthesis of a processable halide perovskite quantum dot–MOF composite by post-synthetic metalation. *Journal of Materials Chemistry A* **2019**, *7*, 21106–21111.

(14) Zhao, Q.; Hazarika, A.; Schelhas, L. T.; Liu, J.; Gaulding, E. A.; Li, G.; Zhang, M.; Toney, M. F.; Sercel, P. C.; Luther, J. M. Size-dependent lattice structure and confinement properties in CsPbI3 perovskite nanocrystals: negative surface energy for stabilization. *ACS Energy Letters* **2019**, *5*, 238–247.

(15) Cheng, O. H.-C.; Qiao, T.; Sheldon, M.; Son, D. H. Size-and temperature-dependent photoluminescence spectra of strongly confined CsPbBr 3 quantum dots. *Nanoscale* **2020**, *12*, 13113–13118.

(16) Doherty, T. A.; Winchester, A. J.; Macpherson, S.; Johnstone, D. N.; Pareek, V.; Tennyson, E. M.; Kosar, S.; Kosasih, F. U.; Anaya, M.; Abdi-Jalebi, M., et al. Performance-limiting nanoscale trap clusters at grain junctions in halide perovskites. *Nature* **2020**, *580*, 360–366.

(17) Brown, A. A.; Vashishtha, P.; Hooper, T. J.; Ng, Y. F.; Nutan, G. V.; Fang, Y.; Giovanni, D.; Tey, J. N.; Jiang, L.; Damodaran, B., et al. Precise Control of CsPbBr3 Perovskite Nanocrystal Growth at Room Temperature: Size Tunability and Synthetic Insights. *Chemistry of Materials* **2021**, *33*, 2387–2397.

(18) Lim, S.; Lee, G.; Han, S.; Kim, J.; Yun, S.; Lim, J.; Pu, Y.-J.; Ko, M. J.; Park, T.; Choi, J., et al. Monodisperse Perovskite Colloidal Quantum Dots Enable High-Efficiency Photovoltaics. *ACS Energy Letters* **2021**, *6*, 2229–2237.

(19) Santori, C.; Fattal, D.; Vučković, J.; Solomon, G. S.; Yamamoto, Y. Indistinguishable photons from a single-photon device. *nature* **2002**, *419*, 594–597.

(20) Gschrey, M.; Thoma, A.; Schnauber, P.; Seifried, M.; Schmidt, R.; Wohlfeil, B.; Krüger, L.; Schulze, J.-H.; Heindel, T.; Burger, S., et al. Highly indistinguishable photons from deterministic quantum-dot microlenses utilizing three-dimensional in situ electron-beam lithography. *Nature Communications* **2015**, *6*, 1–8.

(21) Zehtabi-Oskuie, A.; Jiang, H.; Cyr, B. R.; Rennehan, D. W.; Al-Balushi, A. A.; Gordon, R. Double nanohole optical trapping: dynamics and protein-antibody co-trapping. *Lab on a Chip* **2013**, *13*, 2563–2568.

(22) Jensen, R. A.; Huang, I.-C.; Chen, O.; Choy, J. T.; Bischof, T. S.; Lončar, M.; Bawendi, M. G. Optical trapping and two-photon excitation of colloidal quantum dots using bowtie apertures. *ACS Photonics* **2016**, *3*, 423–427.

(23) Jiang, Q.; Roy, P.; Claude, J.-B.; Wenger, J. Single Photon Source from a Nanoantenna-Trapped Single Quantum Dot. *Nano Letters* **2021**, *21*, 7030–7036.

(24) Harankahage, D.; Cassidy, J.; Yang, M.; Porotnikov, D.; Williams, M.; Kholmicheva, N.; Zamkov, M. Quantum Computing with Exciton Qubits in Colloidal Semiconductor Nanocrystals. *The Journal of Physical Chemistry C* **2021**, *125*, 22195–22203.

(25) de Weerd, C.; Gomez, L.; Zhang, H.; Buma, W. J.; Nedelcu, G.; Kovalenko, M. V.; Gregorkiewicz, T. Energy transfer between inorganic perovskite nanocrystals. *The Journal of Physical Chemistry C* **2016**, *120*, 13310–13315.

(26) Du, X.; Wu, G.; Cheng, J.; Dang, H.; Ma, K.; Zhang, Y.-W.; Tan, P.-F.; Chen, S. High-quality CsPbBr 3 perovskite nanocrystals for quantum dot light-emitting diodes. *RSC Advances* **2017**, *7*, 10391–10396.

(27) Ravindranath, A. L.; Shariatdoust, M. S.; Mathew, S.; Gordon, R. Colloidal lithography double-nanohole optical trapping of nanoparticles and proteins. *Optics Express* **2019**, *27*, 16184–16194.

(28) Sharifi, Z.; Dobinson, M.; Hajisalem, G.; Shariatdoust, M. S.; Frencken, A. L.; van Veggel, F. C.; Gordon, R. Isolating and enhancing single-photon emitters for 1550 nm quantum light sources using double nanohole optical tweezers. *The Journal of Chemical Physics* **2021**, *154*, 184204.

(29) Alizadehkhaledi, A.; Frencken, A. L.; van Veggel, F. C.; Gordon, R. Isolating nanocrystals with an individual erbium emitter: A route to a stable single-photon source at 1550 nm wavelength. *Nano Letters* **2019**, *20*, 1018–1022.

(30) Jauffred, L.; Oddershede, L. B. Two-photon quantum dot excitation during optical trapping. *Nano Letters* **2010**, *10*, 1927–1930.

(31) Berthelot, J.; Aćimović, S. S.; Juan, M. L.; Kreuzer, M. P.; Renger, J.; Quidant, R. Three-dimensional manipulation with scanning near-field optical nanotweezers. *Nature Nanotechnology* **2014**, *9*, 295–299.

(32) Chen, C.; Juan, M. L.; Li, Y.; Maes, G.; Borghs, G.; Van Dorpe, P.; Quidant, R. Enhanced optical trapping and arrangement of nano-objects in a plasmonic nanocavity. *Nano Letters* **2012**, *12*, 125–132.

(33) Kotnala, A.; Gordon, R. Quantification of high-efficiency trapping of nanoparticles in a double nanohole optical tweezer. *Nano Letters* **2014**, *14*, 853–856.

(34) Wheaton, S.; Gordon, R. Molecular weight characterization of single globular proteins using optical nanotweezers. *Analyst* **2015**, *140*, 4799–4803.

(35) Hacohen, N.; Ip, C. J.; Gordon, R. Analysis of egg white protein composition with double nanohole optical tweezers. *ACS Omega* **2018**, *3*, 5266–5272.

(36) Brus, L. Electronic wave functions in semiconductor clusters: experiment and theory. *The Journal of Physical Chemistry* **1986**, *90*, 2555–2560.

(37) Yang, R. X.; Tan, L. Z. Understanding size dependence of phase stability and band gap in CsPbI3 perovskite nanocrystals. *The Journal of Chemical Physics* **2020**, *152*, 034702.

(38) Wu, J.; Xiang, D.; Gordon, R. Monitoring gold nanoparticle growth in situ via the acoustic vibrations probed by four-wave mixing. *Analytical Chemistry* **2017**, *89*, 2196–2200.

(39) Lovett, B. W.; Reina, J. H.; Nazir, A.; Briggs, G. A. D. Optical schemes for quantum computation in quantum dot molecules. *Physical Review B* **2003**, *68*, 205319.

(40) Protesescu, L.; Yakunin, S.; Bodnarchuk, M. I.; Krieg, F.; Caputo, R.; Hendon, C. H.; Yang, R. X.; Walsh, A.; Kovalenko, M. V. Nanocrystals of Cesium Lead Halide Perovskites (CsPbX3, X = Cl, Br, and I): Novel Optoelectronic Materials Showing Bright Emission with Wide Color Gamut. *Nano Letters* **2015**, *15*, 3692–3696.

(41) Becker, M. A. et al. Bright triplet excitons in caesium lead halide perovskites. *Nature* **2018**, *553*, 189–193.

(42) Nair, S. V.; Takagahara, T. Theory of exciton pair states and their nonlinear optical properties in semiconductor quantum dots. *Physical Review B* **1997**, *55*, 5153.

(43) Xue, J.; Wang, R.; Chen, L.; Nuryyeva, S.; Han, T.-H.; Huang, T.; Tan, S.; Zhu, J.; Wang, M.; Wang, Z.-K., et al. A small-molecule "charge driver" enables perovskite quantum dot solar cells with efficiency approaching 13%. *Advanced Materials* **2019**, *31*, 1900111.

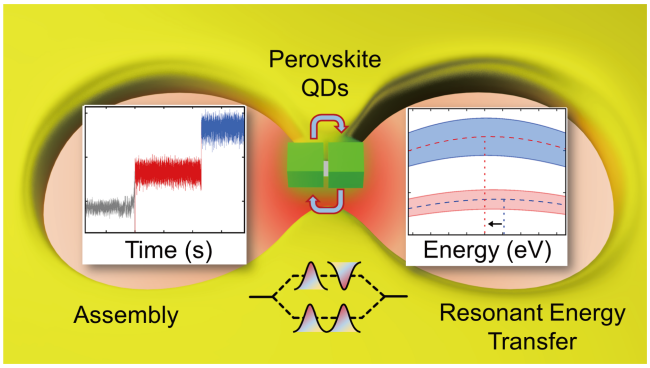

Figure 4: TOC Graphic